Available online at www.sciencedirect.com
ScienceDirect
Surface & Coatings Technology 202 (2008) 3088–3093
SURFACE & COATINGS TECHNOLOGY
www.elsevier.com/locate/surfcoat

Effect of nitrogen-incorporation on structure, properties and performance of magnetron sputtered CrB_2

K.P. Budna [a], P.H. Mayrhofer [b], J. Neidhardt [c], É. Hegedüs [d], I. Kovács [d], L. Tóth [d], B. Pécz [d], C. Mitterer [b,*]

[a] Materials Center Leoben Forschung GmbH, Roseggerstraße 12, A-8700 Leoben, Austria
[b] Department of Physical Metallurgy and Materials Testing, University of Leoben, Franz-Josef-Straße 18, A-8700 Leoben, Austria
[c] Christian Doppler Laboratory for Advanced Hard Coatings, Department of Physical Metallurgy and Materials Testing, University of Leoben, Franz-Josef-Straße 18, A-8700 Leoben, Austria
[d] MFA Research Institute for Technical Physics and Materials Science, Konkoly-Thege u. 29-33, H-1121 Budapest, Hungary

Received 9 July 2007; accepted in revised form 9 November 2007
Available online 21 November 2007

Abstract

Transition metal (TM) boron nitrides are promising candidates for protective coatings with self-lubricating abilities as they can combine properties of TM diborides with the lubricity of hexagonal boron nitride (h-BN). Here, we report on Cr–B–N coatings prepared by unbalanced DC magnetron sputtering of a CrB_2 target in argon/nitrogen atmosphere at 450 °C. By varying the nitrogen partial pressure (p_{N_2}) between 0 and 64% of the total pressure ($p_{Ar}+p_{N_2}$), the N-content in our coatings could be increased from 0 to 47 at.%. The results obtained from X-ray diffraction, transmission electron microscopy and X-ray photoelectron spectroscopy show that for $p_{N_2} \leq 11\%$ a CrB_2-based structure type develops, whereas with increasing p_{N_2} the microstructure becomes then X-ray amorphous and finally CrN is detected as the sole crystalline constituent. With increasing p_{N_2} from 0 to 11%, the hardness and indentation modulus rapidly decrease from 40.6 and 397 GPa for CrB_2 to 13.4 and 108 GPa for $CrB_{2.0}N_{0.5}$. All coatings investigated yield only a moderate friction coefficients between 0.5 and 0.7. Based on detailed high-resolution TEM studies, we can conclude that the missing h-BN based lubricity is due to a lack of a significant long-range order.

Keywords: Magnetron sputtering; Cr–B–N; Microstructure; XRD; TEM

1. Introduction

Protective thin coatings improving the mechanical and tribological performance of tools and components are of increasing importance for industrial applications. This is based on their excellent properties like high corrosion resistance, high thermal stability and favourable friction and wear behaviour. For automotive components like piston rings, wear resistant coatings with low friction coefficients or even self-lubricating ability are desired to e.g., decrease fuel consumption [1].

Candidates for self-lubricating coatings are transition metal boron nitrides (TM–B–N), as they could combine the properties of transition metal (TM) diborides with those of hexagonal boron nitride (h-BN). For example, TiB_2 and CrB_2 are well known for their high hardness and excellent oxidation resistance up to 900 °C in ambient air [2]. h-BN on the other hand is a common solid-lubricant due to its easily activated hexagonal shear systems with possible application temperatures up to 770 °C [2]. Consequently, TM–B–N type coatings are thoroughly investigated, like Zr–B–N [3,4], Ti–B–N [5–11] and Cr–B–N [12–18]. Although there is conclusive evidence that h-BN can be formed in TM–B–N thin coatings [19], their reported lack of self-lubricating properties remains largely unexplained.

Thus, a detailed characterisation of chemical composition as well as bonding- and microstructure of magnetron sputtered Cr–B–N coatings is presented here and correlated to their mechanical and tribological properties, in order to provide an explanation for the missing lubricity of BN containing coatings.

* Corresponding author. Tel.: +43 3842 402 4220; fax: +43 3842 402 4202.
E-mail address: christian.mitterer@mu-leoben.at (C. Mitterer).

0257-8972/$ - see front matter © 2007 Elsevier B.V. All rights reserved.
doi:10.1016/j.surfcoat.2007.11.009

2. Experimental details

Cr–B–N coatings were synthesized by unbalanced reactive magnetron sputtering of a sintered CrB_2 target (Chemco GmbH, Bad Soden-Salmünster, Germany, 99.5% pure, ∅ 150×6 mm) in an Ar/N_2 atmosphere (99.999% pure) in a laboratory-scale unbalanced DC magnetron sputtering system [19] with a base pressure $<1\times10^{-3}$ Pa. Mirror-polished silicon (100) ($20\times7\times0.45$ mm^3) and AISI M2 high-speed steel disks (DIN 1.3343, ∅ 40×10 mm) with a hardness of 65 HRC were used as substrates. Prior to mounting on the substrate holder parallel to the target surface at a distance of 10 cm above the target (see reference [20] for more details), the substrates were ultrasonically pre-cleaned in acetone and ethanol. The target was pre-sputtered for 5 min at a current of 1.5 A in Ar atmosphere at 0.4 Pa, and the substrates were ion-etched using an Ar glow discharge with −1250 V at 2.6 Pa. During deposition, the substrate temperature as well as total gas pressure ($p_{Ar}+p_{N_2}$) was kept constant at 450 °C and 0.4 Pa as controlled by a calibrated thermocouple as well as a capacitive gauge, respectively, while the nitrogen partial pressure p_{N_2} was varied stepwise from 0 to 64%. The sputter power density on the target was set to ~4 W/cm^2 and a constant substrate bias of −50 V was applied. The 60 min deposition time results in a thickness of ~4.5 μm for coatings synthesized at lower $p_{N_2}<32\%$ while the increasing target poisoning at higher p_{N_2} reduces the deposition rate by almost 60%.

The composition of selected coatings as well as their chemical bonding structure was determined by X-ray photoelectron spectroscopy (XPS) performed with an Omicron Multiprobe analysis system using a monochromized Al Kα X-ray beam with a resolution of <0.2 eV. The composition was determined after 2500 eV Ar ion sputter cleaning for 40 min using calibrated sensitivity factors for the specific elements [21]. The core level for bonding evaluation were recorded without initial sputter cleaning to avoid structural rearrangement and subsequently fitted using the Unifit Software package [22].

Microstructural investigations were performed by Bragg-Brentano X-ray diffraction (XRD, Siemens D500) using Cu Kα radiation. The so obtained patterns were simulated by Rietveld analysis using the Topas 2.1 software package. A Philips CM20 transmission electron microscope (TEM) operated at 200 kV was used for studies of the average particle size utilizing bright- and dark-field modes. The overall crystal structure was investigated by selected area electron diffraction (SAED) patterns. On selected sample cross-sections, high-resolution transmission electron microscopy (HRTEM) was conducted with a JEOL 3010 operating at 300 kV (ideal point-to-point resolution of 0.17 nm). Some high-resolution micrographs were first Fourier-transformed using the FFT (Fast Fourier Transformation) routine included in GATAN DigitalMicrograph software package and then filtered by a ring mask, thus selecting a range of lattice spacing values. After back-transformation of the filtered FFT, these selected spacings are significantly enhanced on the processed image irrespective of their direction. The cross-sectional samples for TEM analysis were mechanically ground, polished and subsequently thinned by ion milling at 10 keV by Ar^+ ions. In order to minimize the ion beam damage, the energy was decreased to 3 keV in the final stage.

Indentation modulus (E) and universal plastic hardness (H) of our coatings on steel substrates were determined from the loading and unloading segments during 25 computer-controlled micro-indentations (Fischerscope H100C). The maximum load applied to the Vickers indenter was 30 mN for the thicker coatings deposited at low N_2 partial pressures and 15 mN for those synthesized at partial pressures higher than 43% to limit the indentation depth to a maximum of 10% of the coating thickness. Ball-on-disk dry sliding tests in ambient atmosphere (humidity ~45%) of the coated steel disks were conducted at room temperature using a CSM tribometer and sintered alumina balls (∅=6 mm) as counterparts. A constant velocity of 10 cm/s, a sliding distance of 300 m and a wear track radius of 5 mm were used. The resulting wear tracks were analyzed by white-light-optical profilometry (Veeco NT 1100).

3. Results and discussion

3.1. Chemical composition

Fig. 1 (a) shows the coating composition in the simplified Cr–B–N triangular phase diagram, where major ternary phase fields like Cr+CrB_2+CrN (I), B+CrB_2+BN (II), N+BN+CrN (III), and CrN+BN+CrB_2 (IV) are indicated, while the impurity level for O and C in the bulk is below 1 at.%. With increasing N_2 partial pressure, the coating composition changes from the single phase CrB_2 via the ternary CrN+BN+CrB_2 phase field to the quasi-binary CrN–BN tie-line at the highest partial pressure of 64%. The reliability of the measurement, e.g., in terms of the calibrated XPS sensitivity factors is indicated by the fairly constant Cr/B ratio of 0.47±0.04, see Table 1. The rapidly increasing supply of activated nitrogen (ions and

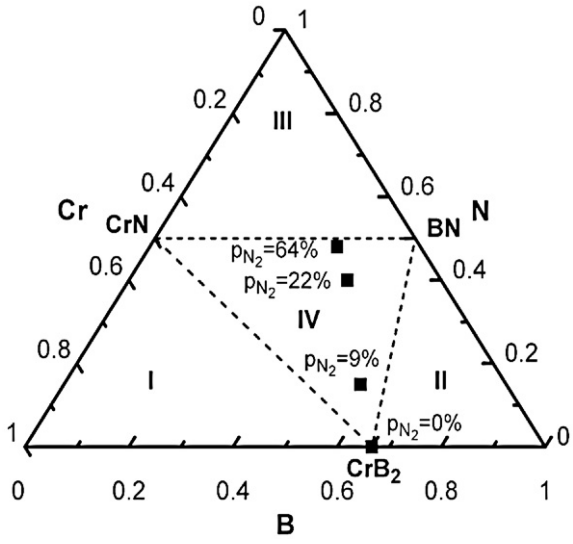

Fig. 1. Chemical composition of the deposited coatings within the simplified Cr–B–N triangular phase diagram (after [12]) with indicated major ternary phase fields like Cr+CrB_2+CrN (I), B+CrB_2+BN (II), N+BN+CrN (III), and CrN+BN+CrB_2 (IV).

Table 1
Composition of the Cr–B–N coatings for various p_{N_2} determined by XPS alongside with the calculated equilibrium ratios of the main constituents (CrB_2, CrN, BN)

p_{N_2} (%)	Composition (at.%)				Calculated phase composition (mol%)		
	Cr	B	N	Cr/B	CrB_2	CrN	BN
0	33.7	66.3	0	0.51	100	0	0
9	28.1	57.4	14.5	0.49	62.0	11.6	26.4
22	17.9	42.3	39.8	0.42	14.5	23.9	61.6
64	16.3	36.3	47.4	0.45	3.5	29.7	66.8

radicals originating from the plasma) with increasing partial pressure leads to a sharp increase in N concentration and, thus, the formation of CrN and BN on the expense of CrB_2. This is also corroborated by the much larger Gibbs free energy of −117.1 kJ/mol (CrN) and −250.5 kJ/mol (BN) of the nitrides compared to just −94.1 kJ/mol (CrB_2) for the boride [23].

Since non-equilibrium thermodynamic growth conditions are inherent to PVD thin film growth, the equilibrium phase composition purely derived from the respective elemental concentrations, as shown in Table 1, might be offset. Thus, XPS core level spectra of the respective elements were recorded to qualitatively support the presented trends by the observed chemical shift characteristic for a certain bonding environment. The spectra were recorded from as-deposited samples without any initial sputter-cleaning to avoid unintentional rearrangement of the bonding states. Fig. 2 shows the respective Cr 2p, B 1s and N 1s spectra together with the reported binding energies of the contributing main bonding configurations [24,25]. Oxygen-related contributions can be detected for Cr and B at higher binding energies due to its high electro-negativity indicating surface oxidation, which do, however, not overlap with B, Cr or N related features. Besides Cr–O, Cr–B and Cr–N bonding states can be detected for the Cr 2p duplet (1/2 and 3/2) according to references for CrB_2 and CrN as well as Cr_2N [24,25] (Fig. 2 (a)). The small difference between the two binding energies allows for an indication of a shift from a boride to a nitride-dominated environment with increasing partial pressure. Also for B 1s (Fig. 2 (b)) B–N and B–Cr bonding states are present. At low partial pressures only one peak at ~188 eV could be detected, which corresponds fairly well to CrB_2 at 187.5 eV [24]. With increasing N_2 fraction, the B–N related contribution emerges at 190.5 eV (BN ~191 eV [24]) indicating the already mentioned formation of BN. By additional investigations of the N 1s core levels (Fig. 2 (c)), a corresponding tendency can be found. With increasing N content in the Cr–B–N coatings, a broad feature at ~397.6 eV emerges with an increasing shoulder towards lower binding energies, due to the overlap of N–Cr and N–B contributions at approximately 396.7 and 398.1 eV [15], respectively. In summary, without N_2 in the discharge exclusively Cr–B bonds are present, while at increasing p_{N_2}, contributions from Cr–N as well as B–N emerge until no Cr–B bonds can be detected any more by XPS for the highest p_{N_2} of 64%. This corroborates the already presented notion (Table 1) that the boride dominated structure fully transforms into the CrN+BN dual phase, as already suggested by the stoichiometry and the phase diagram.

3.2. Structure and morphology

X-ray diffractograms of the Cr–B–N coatings on Si substrates, with their (200) reflection at 32.9° 2θ, are presented in Fig. 3 as a function of p_{N_2}. The standard 2θ positions for cubic CrN (JCPDS #11-0065) and hexagonal CrB_2 (JCPDS #34-0369) are added. For the coating deposited without nitrogen, only the rather narrow reflections at 29.8 and 61.3° 2θ attributable to (001) and (002) CrB_2 can be detected suggesting a strongly textured film growth as reported also for TiB_2 in Ref. [26] with a rather large domain size. With increasing N-content, the CrB_2 reflections decrease in intensity and broaden. The additional (100) and (101) reflections for CrB_2 at 34.9 and 46.5° 2θ for the coatings prepared with p_{N_2}=9 and 11%, respectively, indicate that

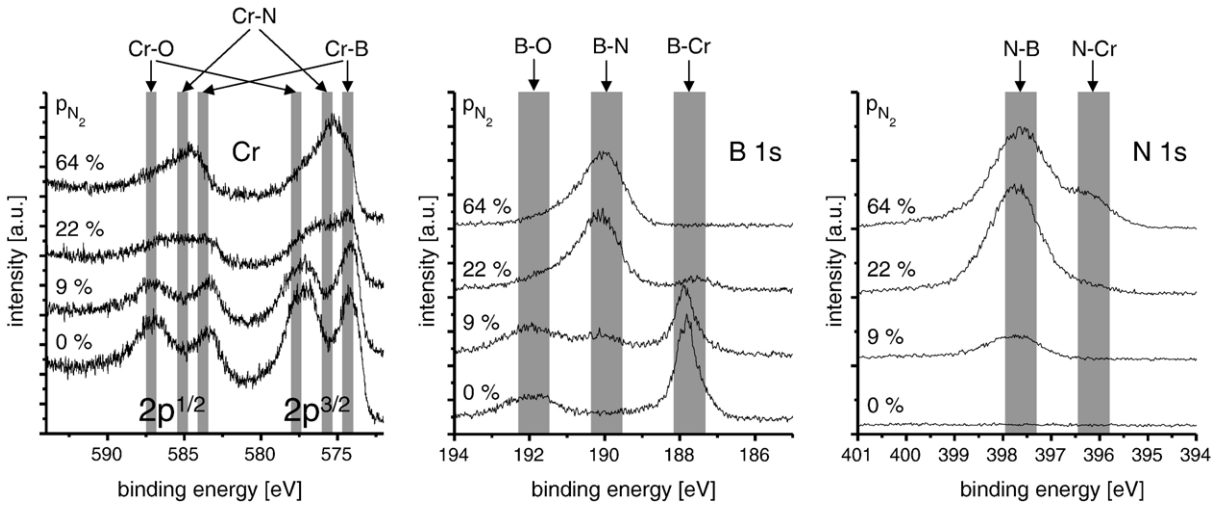

Fig. 2. XPS Cr 2p, B 1s and N 1s core level spectra of Cr–B–N-coatings synthesized at various p_{N_2} fractions. The grey regions indicate binding energies of the respective reference compounds [24,25].

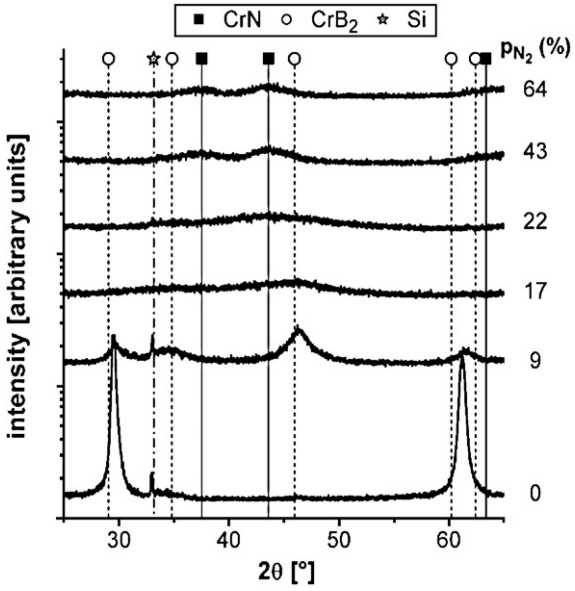

Fig. 3. XRD patterns of Cr–B–N coatings on Si(100) substrates with increasing p_{N_2}.

the preferred growth orientation of CrB_2 is suppressed and the crystallinity deteriorates substantially. For the Cr–B–N coatings, deposited between 17 and 33% p_{N_2}, an X-ray amorphous structure evolves showing a broad low intensity coating reflection ranging from 37–58° 2θ. For coatings prepared at p_{N_2}>43%, reflections attributed to CrN (111), (200), and (220) can be detected. Consequently, the evolution of crystalline phases of the Cr–B–N coatings can be subdivided into CrB_2 dominated (for $p_{N_2} \leq 11\%$), X-ray amorphous (for p_{N_2} between 17–43%), and CrN dominated (for p_{N_2}>43%). Quantitative Rietveld analysis conducted for representative Cr–B–N coatings, deposited at p_{N_2}=9 or 64%, respectively, yield an average domain size of 2–5 nm.

TEM dark-field images of CrB_2 and three representative Cr–B–N (p_{N_2}=9, 22, 64%) coatings are displayed in Figs. 4 (a), (b), (c) and (d), respectively. The small inserts show the corresponding SAED patterns and indicate a good agreement to the conducted XRD investigations. The CrB_2 coating (Fig. 4 (a)) exhibits a columnar growth with diameters of ~10 nm comparable to Ref. [27,28]. The SAED pattern indicates the hexagonal CrB_2 phase and due to the strong texture an almost single-crystalline pattern. For the Cr–B–N coatings, the dark-field images show a pronounced reduction of the crystallite size and suppression of the columnar growth with increasing p_{N_2}. Hexagonal CrB_2 can still be found for the coating prepared at p_{N_2}=9%. The broad SAED rings as well as the featureless micrograph at p_{N_2}=22% corroborate the amorphous nature of the coatings synthesized at intermediate N_2 fractions. For the coating deposited at p_{N_2}=64% (Fig. 4 (d)), the CrN structure evolves which is consistent with the SAED pattern.

For all coatings investigated, no laminar structures or small crystals of h-BN could be identified. Based on the TEM investigations, we can conclude that with increasing p_{N_2} the

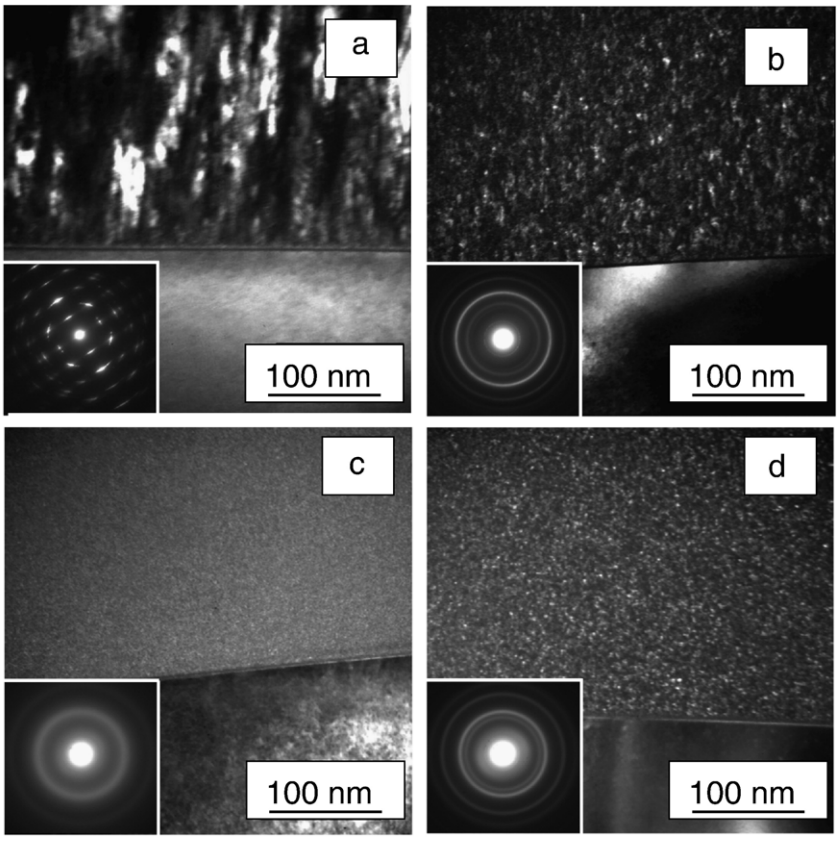

Fig. 4. Cross-sectional dark-field TEM micrographs of Cr–B–N coatings deposited at (a) p_{N_2}=0%, (b) 9%, (c) 22%, and (d) 64% (d), alongside with their respective SAED patterns taken near the interface.

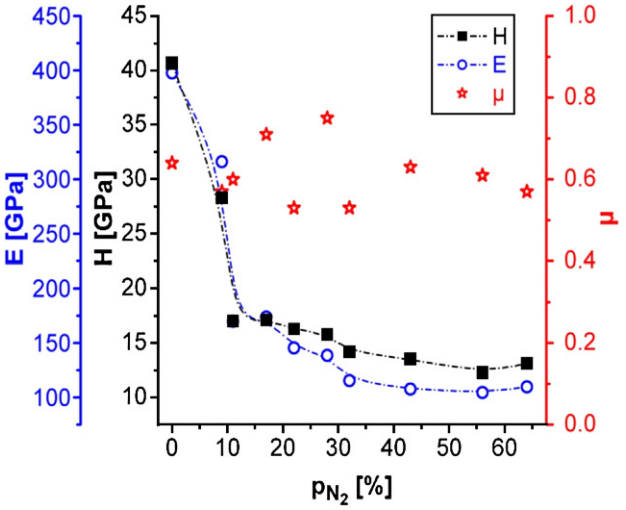

Fig. 5. Hardness and elastic modulus, obtained by micro-indentation, as well as friction coefficients obtained for Cr–B–N coatings as a function of p_{N_2}. The total error for H and E as obtained from the standard deviation of the indentation data is app. ±5%.

coating structure changed from columnar to equiaxed. For p_{N_2} between 17 and 43%, an amorphous structure can be found, and for p_{N_2} > 43%, the structure is dominated by CrN, in agreement to the XRD studies, as well as amorphous fractions — most likely BN, as indicated by XPS. A detailed report on the respective TEM investigations can be found in [29].

3.3. Mechanical and tribological properties

The indentation modulus (E) and hardness (H) of the Cr–B–N coatings are presented in Fig. 5 as a function of p_{N_2}. A maximum in hardness and modulus of 40.6 and 397 GPa, respectively, is obtained for the CrB_2 coating. Very high hardness values for borides are reported due to their nanocolumnar structure and the strong covalent bonds within the B network, see, e.g., Ref. [26] for TiB_2 as well as Ref. [28] for CrB_2. With increasing nitrogen content, hardness and modulus of the Cr–B–N coatings rapidly decrease via intermediate values of 26 and 300 GPa at p_{N_2} = 9% down to 14 and 120 GPa for p_{N_2} > 30%. This drop in mechanical properties coincides with the preferred formation of a large fraction of amorphous BN phase as indicated by XPS (see Table 1) and TEM, presumably with less advantageous mechanical properties. For a lower N_2 fraction of 9%, ~26 mol% amorphous BN is assumed to be formed surrounding the small equiaxed CrB_2 crystallites resulting in intermediate hardness values. With increasing p_{N_2}, the BN fraction saturates rapidly at values ≥60 mol% giving rise to a further deterioration of the mechanical properties. Hereby, the coating structure changes from completely amorphous (p_{N_2} ~ 22%) to an almost quasi-binary structure built of nanocrystalline CrN embedded in an amorphous BN matrix. The low mass density of BN hereby results in an even higher volume fraction of rather soft amorphous BN, which does not provide a significant resistance to plastic deformation.

Surprisingly, the tribological investigation of Cr–B–N coatings shows only minor differences of their friction coefficients (μ), which are rather constant at ~0.6±0.15 (see Fig. 5) regardless the amount of BN phase fraction. Even for coatings which contain dominantly BN (obtained by XPS, see Table 1), no low-friction effect could be observed. These results suggest that the formed BN phase lacks morphology and/or structure which could support shearing and, hence, lower the friction coefficient. To illuminate this, the high N-containing coating (N ~ 47 at.%, p_{N_2} = 64%), which shows the highest amount of BN phase (~67 mol%), was investigated by HRTEM. Fig. 6 (a) and (b) show Fourier-transformed cross-sectional HRTEM images utilizing the CrN and BN lattice spacing, respectively (see Ref. [29] for details). The morphology of this coating can be described as nanocomposite, where small grains (2–5 nm) of cubic CrN (Fig. 6 (a)) are embedded in a large fraction of predominantly amorphous BN matrix (Fig. 6 (b)). Within the amorphous BN matrix, a hexagonal lattice can only be identified for a few atomic layers, which have, furthermore, no preferential orientation [29]. Consequently, these sub-5-nm crystalline h-BN domains do not support shearing in a macroscopic tribological contact due to their small lateral extension and random orientation.

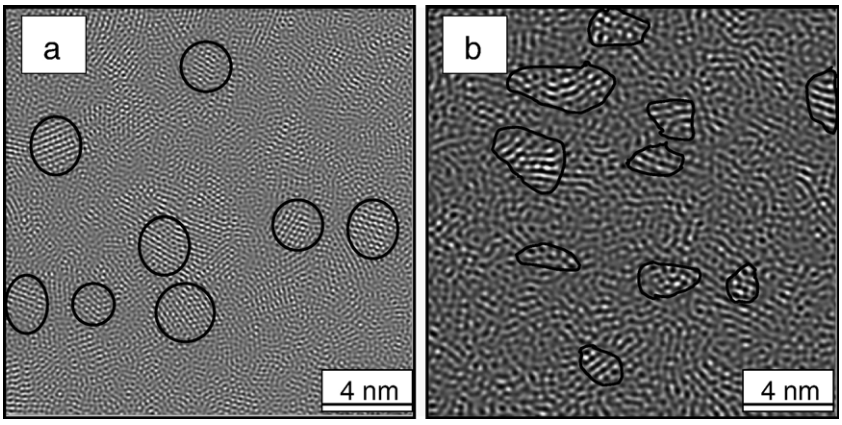

Fig. 6. Digitally processed HRTEM images showing the same area of a cross-sectional specimen for a Cr–B–N coating deposited at p_{N_2} = 64%. Fourier-filtered images using a ring mask enhancing (a) CrN (d = 0.20–0.26 nm) and (b) BN (d = 0.28–0.36 nm) spacings. The black lines are guides to the eye helping to identify coherent particles of the phases.

4. Conclusions

Cr–B–N coatings were synthesised by reactive unbalanced magnetron sputtering using a CrB_2 target in an argon/nitrogen atmosphere. By increasing the nitrogen partial pressure p_{N_2} from 0 to 64% of the total pressure ($p_{Ar}+p_{N_2}$), the N content within the coatings could be increased to ~47 at.%, since Cr and B nitrides are thermodynamically favourable over CrB_2. Thus, the coating composition changes from the single CrB_2 phase via the ternary CrN–BN–CrB_2 phase field to a binary CrN–BN phase mixture. Owing to the large amount of B, predominantly amorphous BN is formed as soon as nitrogen is present in the discharge, which saturates at a phase fraction ≥62 mol% for $p_{N_2} \geq 22\%$. As to the crystalline constituents, the CrB_2 coating, prepared with $p_{N_2}=0\%$, exhibits a columnar growth with (001) preferred orientation and hardness and indentation modulus of 40.6 and 397 GPa, respectively. With increasing N content, the columnar structure is suppressed by re-nucleation processes and for p_{N_2} between 17 and 43% an amorphous structure evolves. For $p_{N_2}>43\%$, crystalline CrN with diameters of 2–5 nm can be detected by X-ray diffraction, selected area electron diffraction, and transmission electron microscopy. Due to the increasing volume fraction of amorphous BN in the Cr–B–N coatings, their hardness and indentation modulus rapidly decreases with increasing N content to values below 17.1 and 174 GPa for $p_{N_2} \geq 17\%$.

Although a large amount of BN is present in the Cr–B–N coatings prepared at $p_{N_2} \geq 22\%$, no solid-lubricant low-friction effect could be observed. All coatings show a friction coefficient of $\sim 0.6 \pm 0.15$, independent of their chemical composition and microstructure. Fourier-transformed high-resolution transmission electron microscopy studies showed that the formed BN phase is highly distorted with no preferred orientation and hexagonal domains extending only over a few atomic layers. Consequently, this BN phase is not able to develop a low-friction effect by easy shearing during tribological contacts.

Acknowledgments

This work was financially supported by the European Union within the NAPILIS Specific Targeted Research Project (contract NMP3 CT 2003 505622). The authors are grateful for the XPS investigations performed by A. Fian (Joanneum Research, Weiz, Austria). J.N. acknowledges financial support by the Christian Doppler Society and the companies Plansee GmbH, Lechbruck, Germany, and Oerlikon Balzers AG, Balzers, Liechtenstein.

References

[1] I. Kvernes, P. Fartum, Thin Solid Films 53 (1978) 259.
[2] R.J. Brotherton, H. Steinberg, Progress in Boron Chemistry, vol.2, Pergamon Press, Oxford, 1970, p. 173.
[3] C. Mitterer, A. Übleis, R. Ebner, Mater. Sci. Eng. A 140 (1991) 670.
[4] E. Brandstetter, C. Mitterer, R. Ebner, Thin Solid Films 210 (1991) 123.
[5] C. Mitterer, P. Rödhammer, H. Störi, F. Jeglitsch, J. Vac Sci. Technol. A 7 (1989) 2646.
[6] C. Mitterer, M. Rauter, P. Rödhammer, Surf. Coat. Technol. 42 (1990) 351.
[7] B. Matthes, E. Broszeit, K.H. Kloos, Surf. Coat. Technol. 43-44 (1990) 721.
[8] L.S. Wen, X.Z. Chen, Q.Q. Yang, Y.Q. Zheng, Y.Z. Chuang, Surf. Eng. 6 (1990) 41.
[9] O. Knotek, F. Jungblut, K. Breidenbach, Vacuum 41 (1990) 2184.
[10] W. Gissler, Surf. Coat. Technol. 68-69 (1994) 556.
[11] P.H. Mayrhofer, C. Mitterer, J.G. Wen, I. Petrov, J.E. Greene, J. Appl. Phys. 100 (2006) 044301.
[12] P. Rogl, J.C. Schuster, Phase Diagrams of Ternary Boron Nitride and Silicon Nitride Systems, ASM, Materials Park, OH, 1992 p. 20.
[13] B. Rother, H. Kappl, Surf. Coat. Technol. 73 (1995) 14.
[14] B. Rother, H. Kappl, Surf. Coat. Technol. 96 (1997) 163.
[15] S.M. Aouadi, F. Namavar, E. Tobin, N. Finnegan, R.T. Haasch, R. Nilchiani, J.A. Turner, S.L. Rohde, J. Appl. Phys. 91 (2002) 1040.
[16] T.Z. Gorishnyy, D. Mihut, S.L. Rohde, S.M. Aouadi, Thin Solid Films 445 (2003) 96.
[17] Y. Sakamaoto, M. Nose, T. Mae, E. Honbo, M. Zhou, K. Nogi, Surf. Coat. Technol. 174-175 (2003) 444.
[18] M. Zhou, M. Nose, K. Nogi, Surf. Coat. Technol. 183 (2004) 45.
[19] T.P. Mollart, M. Baker, J. Haupt, A. Steiner, P. Hammer, W. Gissler, Surf. Coat. Technol. 74 (1995) 491.
[20] P. Losbichler, C. Mitterer, P.N. Gibson, W. Gissler, F. Hofer, P. Warbichler, Surf. Coat. Technol. 94/95 (1997) 297.
[21] J.H. Scofield, J. Electron. Spectrosc. Rel. Phenom. 8 (1976) 129.
[22] http://www.uni-leipzig.de/~unifit/ (accessed May 2007).
[23] HSC 5.11, 2004 HSC Chemistry 5.11, Outokumpu Research Oy, Pori, Finland, 2004.
[24] NIST X-ray Photoelectron Spectroscopy Database, http://srdata.nist.gov/xps/.
[25] C.D Wagner, Handbook of XPS, Physical Electronics Inc., Minnesota, 1995.
[26] P.H. Mayrhofer, C. Mitterer, J.G. Wen, J.E. Greene, I. Petrov, Appl. Phys. Lett. 86 (2005) 131909.
[27] A. Audronis, P.J. Kelly, A. Leyland, A. Matthews, Thin Solid Films 515 (2006) 1511.
[28] A. Audronis, P.J. Kelly, A. Leyland, A. Matthews, Surf. Coat. Technol. 201 (2006) 3970.
[29] É. Hegedűs, I. Kovács, B. Pécz, L. Tóth, K.P. Budna, C. Mitterer, Vacuum 82 (2008) 209.